JACS
JOURNAL OF THE AMERICAN CHEMICAL SOCIETY

Communication

pubs.acs.org/JACS

Beryllium-Free $Rb_3Al_3B_3O_{10}F$ with Reinforced Interlayer Bonding as a Deep-Ultraviolet Nonlinear Optical Crystal

Sangen Zhao,[†] Pifu Gong,[‡,§] Siyang Luo,[‡] Sijie Liu,[†,§] Lina Li,[†] Muhammad Adnan Asghar,[†,§] Tariq Khan,[†,§] Maochun Hong,[†] Zheshuai Lin,[‡] and Junhua Luo*[,†]

[†]Key Laboratory of Optoelectronic Materials Chemistry and Physics, Fujian Institute of Research on the Structure of Matter, Chinese Academy of Sciences, Fuzhou, Fujian 350002, China

[‡]Beijing Center for Crystal R&D, Key Lab of Functional Crystals and Laser Technology of Chinese Academy of Sciences, Technical Institute of Physics and Chemistry, Chinese Academy of Sciences, Beijing 100190, China

[§]University of Chinese Academy of Sciences, Beijing 100049, China

Supporting Information

ABSTRACT: A new beryllium-free borate $Rb_3Al_3B_3O_{10}F$ has been synthesized and characterized by single-crystal X-ray diffraction. It features a framework structure consisting of alveolate $[Al_3(BO_3)_3OF]_\infty$ layers tightly bound via Al−O and Al−F bridged bonds, with the in-layer $[BO_3]^{3-}$ groups in nearly coplanar and aligned arrangement. This compound is transparent down to 200 nm and is phase-matchable with a powder second-harmonic generation efficiency of 1.2 times that of KH_2PO_4. Remarkably, it exhibits a strong interlayer bonding which is about one order larger than that of the benchmark $KBe_2BO_3F_2$, thus no layering tendency was observed during the crystal growth. In addition, it is nonhygroscopic and thermally stable up to ∼1462 K. These attributes make $Rb_3Al_3B_3O_{10}F$ a promising nonlinear optical crystal in the deep-ultraviolet region. First-principles calculations, combined with the anionic group theory, were adopted to rationalize the optical properties.

Nonlinear optical (NLO) materials have attracted continuous intensive attention since the second-harmonic generation (SHG) phenomenon was first observed in 1961.[1] A number of NLO materials, such as β-BaB_2O_4,[2] LiB_3O_5,[3] $KTiOPO_4$,[4] $AgGaS_2$,[5] and $ZnGeP_2$,[6] have been developed and commercially used for NLO applications from ultraviolet region to infrared spectral regions. However, there is still a lack of commercially available NLO materials for the applications in deep-ultraviolet (deep-UV, wavelengths below 200 nm) region. To be optically applicable, a deep-UV NLO material must satisfy several fundamental but rigorous requirements on the structure-directing optical properties: wide transparent window down to the deep-UV region, relatively large SHG response, and sufficient birefringence to achieve phase matching.[7] So far $KBe_2BO_3F_2$ (KBBF)[8] is the sole NLO material that can practically generate deep-UV coherent light by direct SHG process. The KBBF crystal features a layered structure, with NLO-active $[BO_3]^{3-}$ groups in coplanar and aligned arrangement giving rise to a relatively large SHG response and sufficient birefringence.[8c] Unfortunately, its interlayer bonding (dominated by K−F ionic bonds) is so weak that a strong layering tendency occurs in the process of crystal growth; moreover, the constituent beryllium is highly toxic.[8b] Consequently, the production and applications of KBBF are still limited at the laboratory stage, in spite of the great efforts since the discovery of its superior deep-UV NLO performance in 1995.[8a] Therefore, it is in urgent demand to develop the so-called next generation of deep-UV NLO materials, which could preserve the optical merits while overcoming the demerits of KBBF.

To overcome the structural demerits of KBBF, a traditional but effective strategy is to develop similar beryllium borates with reinforced interlayer bonding. The resultant deep-UV NLO materials include $Sr_2Be_2B_2O_7$,[9] $NaBeB_3O_6$, and $ABe_2B_3O_7$ (A = K, Rb),[10] $Na_2CsBe_6B_5O_{15}$,[11] $Na_3Sr_3Be_3B_3O_9F_4$,[12] and $NaCaBe_2B_2O_6F$[13] as well as $Na_2Be_4B_4O_{11}$ and $Li_5Na_5Be_{12}B_{12}O_{33}$.[14] The toxicity of beryllium, however, remains an obstacle to their practical applications. On the other hand, although some beryllium-free borates have been reported as potential deep-UV NLO materials in recent years, very few of them maintain the favorable structural features in KBBF.[15] Recently, our group discovered a new beryllium-free borate, $Li_4Sr(BO_3)_2$,[16] which inherits the structural merits and thus the optical advantages of KBBF. Furthermore, $Li_4Sr(BO_3)_2$ greatly mitigates the layering growth tendency by enhancing the interlayer bonding (via Sr−O bonds) to ∼4.7 times that of KBBF in magnitude.[16]

According to the diagonal relationships of the periodic table of elements, the aluminum element is physically and chemically similar to beryllium element. We thus expect the substitution of Be for Al will create new deep-UV NLO materials with similar structural features. In this work, systematic explorations on the aluminum borate systems led to the discovery of a new beryllium-free borate, $Rb_3Al_3B_3O_{10}F$ (compound **I**). The microscopic structure of this compound preserves the NLO-favarable structural features in KBBF. Furthermore, the bridged Al−O/Al−F bonds enhance the interlayer bonding strength to more than 9.5 times as large as that of KBBF.

Polycrystalline samples of **I** were synthesized by solid-state reaction techniques. High-purity $RbNO_3$ (99.99%), Al_2O_3

Received: December 22, 2014
Published: January 30, 2015

© 2015 American Chemical Society

DOI: 10.1021/ja5128314
J. Am. Chem. Soc. 2015, 137, 2207−2210

(99.99%), H_3BO_3 (99.99%), and RbF (99.99%) were used as received. These raw materials were mixed in stoichiometric proportions and ground thoroughly. The mixture was heated to 773 K at a rate of 20 K h^{-1} and then sintered at this temperature for 24 h. The products were ground thoroughly, heated to 1050 K at a rate of 20 K h^{-1}, and then held at this temperature for 120 h with several intermediate grindings. **I** was obtained as a powder. The phase purity was confirmed by powder X-ray diffraction (XRD) (see Figure 1a). **I** crystals

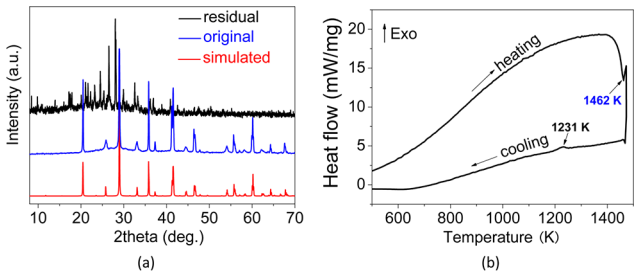

Figure 1. (a) Simulated and experimental XRD patterns and (b) DSC curves for **I**.

(Figure S1) were grown through spontaneous crystallization using the RbF-B_2O_3 flux. Powdered **I**, H_3BO_3 (99.99%), and RbF (99.99%) were mixed at a molar ratio of 1:3:5 in a platinum crucible, melted at 1173 K in a temperature-programmable electric furnace, and then held at this temperature for 24 h to ensure that the melt was homogenized. The melt was then allowed to cool at a rate of 5 K h^{-1} until block **I** crystals crystallized in the melt. The temperature was subsequently decreased to room temperature at a rate of 50 K h^{-1}. Finally, the matrix was washed by hot water, and **I** crystals (Figure S1) were thus obtained. The crystals were not soluble in hot water, indicating that **I** is nonhygroscopic. In the process of crystal growth, no layering growth tendency was observed.

The thermal stability of **I** was investigated by the differential scanning calorimetric (DSC) analysis. As shown in Figure 1b, the DSC data show a sharp endothermic peak around 1462 K in the heating curve and a tiny peak around 1231 K in the cooling curve. In addition, the residues after the DSC analysis gave a powder XRD pattern distinct from that of the original powders (see Figure 1a). These results demonstrate that **I** is an incongruently melting compound with a high decomposition temperature of ~1462 K. Thus, large crystals of **I** can be grown using the flux method and below the decomposition temperature.

The crystal structure of **I** was determined by single-crystal XRD analysis. **I** crystallizes in the trigonal crystal system with an asymmetric space group of $P3_1c$ (detailed crystallographic data in Tables S1−S4). Its crystal structure is composed of alveolate $[Al_3(BO_3)_3OF]_\infty$ layers along the *c* axis bound via Al−O and Al−F bonds to further construct a 3D framework (Figure 2a). Rb^+ cations reside in the cavities of the framework to maintain charge balance: they are all eight-coordinated to form RbO_7F polyhedra with a Rb−F distance of 2.909(3) Å and Rb−O distances ranging from 2.846(11) to 3.252(9) Å. There is only one crystallographically independent boron atom, which is bound to three oxygen atoms to form a $[BO_3]^{3-}$ triangle with B−O distances ranging from 1.348(13) to 1.383(12) Å. The O−B−O angles are in the range of 118.8(9)−121.2(9)°, and the mean value is about 120°,

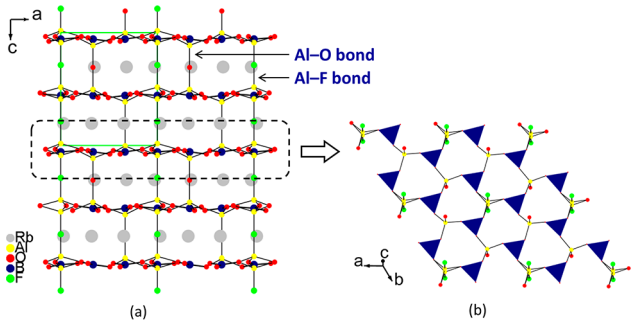

Figure 2. (a) Crystal structure of **I**. (b) $[Al_3(BO_3)_3OF]_\infty$ layer. The interlayer Al−F and Al−O bonds are indicated in (a). Blue triangles in (b) represent $[BO_3]^{3-}$ groups.

indicating that the $[BO_3]^{3-}$ triangle is nearly planar. Al atoms occupy four crystallographically independent sites, and they are all four-coordinated to form AlO_4 or AlO_3F tetrahedra with Al−O and Al−F distances in the ranges of 1.704(15)−1.764(8) Å and 1.71(5)−1.75(5) Å, respectively. Each AlO_4 or AlO_3F tetrahedron is linked to three neighboring $[BO_3]^{3-}$ triangles by sharing its three basal oxygen atoms to further form an alveolate [3, 3] $[Al_3(BO_3)_3OF]_\infty$ layer in the *ab*-plane, which has all $[BO_3]^{3-}$ groups in nearly coplanar and aligned arrangement (Figure 2b). The rest apical O/F atoms of AlO_4/AlO_3F tetrahedra alternately point upward and downward from the $[Al_3(BO_3)_3OF]_\infty$ layer to serve as interlayer bridges. The results of bond valence calculations[17] (Rb, 1.09; Al, 3.05−3.20; B, 3.08; O, −2.03−-2.10; F, −1.23) indicate that the Rb, Al, B, O, and F atoms are in oxidation states of +1, +3, +3, −2, and −1, respectively.

It is interesting to compare the layered structural features in KBBF, $Li_4Sr(BO_3)_2$, and **I** to illustrate their structural evolution (see Figure S2). They all have similar layered structural units that afford favorable, aligned arrangement of $[BO_3]^{3-}$ groups, indicating that they are likely to share the optical advantages of KBBF. Nevertheless, they have distinct interlayer connections. Compared to the weak K−F bonds in KBBF and the relatively stronger Sr−O bonds in $Li_4Sr(BO_3)_2$, the Al−O and Al−F bonds in **I** provide the stongest connection between the layered structural units. We rationalized this point by evaluating the interlayer electrostatic force of interactions, given that the interlayer bonds (Sr−O, Al−O, and Al−F) are basically ionic. According to Coulomb's law,[18] the magnitude of the electrostatics force of interaction can be calculated using eq 1:

$$|F| = \frac{k_e|q_1q_2|}{r^2} \quad (1)$$

where k_e is the electrostatic constant, q_1 and q_2 are the magnitude of the two point charges, respectively, and r is the separation distance between point charges. As shown in Table 1, owing to the relatively large charge magnitude and short bond lengths, the calculated $|F_{Al-O}|$ and $|F_{Al-F}|$ are larger than 15.9 × $|F_{KBBF}|$ and 9.5 × $|F_{KBBF}|$, respectively. It is worth noting that the interaction magnitude of Al−O bonds should be even larger than the calculated values, since the Al−O bonds are virtually to some degree covalent. All in all, the overall interlayer bonding in **I** is at least larger than 9.5 × KBBF (in comparison, $Li_4Sr(BO_3)_2$ ~4.7 × KBBF). In our preliminary experiments, the as-grown **I** crystals are of block shape, and no layering growth tendency was observed.

DOI: 10.1021/ja5128314
J. Am. Chem. Soc. 2015, 137, 2207−2210

Table 1. Comparisons of the Interlayer Bonding for KBBF, $Li_4Sr(BO_3)_2$, and I

species	bonds	lengths (Å)	q_1[a]	q_2[a]	$\|F\|$[b]
KBBF[c]	K−F	2.755	1	1	1
$Li_4Sr(BO_3)_2$[d]	Sr−O	2.533	1.99	1.99	4.7
I[e]	Al2−F1	1.750	3.12	1.23	9.5
	Al1−F1	1.710	3.20	1.23	10.2
	Al3−O1	1.717	3.05	2.03	15.9
	Al4−O1	1.704	3.14	2.03	16.7

[a]In multiples of 1.602×10^{-19} C. [b]In multiples of $|F_{KBBF}|$. [c]Data from ref 8a. [d]Data from ref 16. [e]This work.

Since **I** crystallizes in an asymmetric space group, it is expected to be NLO-active. We carried out SHG measurements by the Kurtz−Perry method[19] with an incident laser of 1064 nm. As shown in Figure 3a, the SHG intensities for **I** increase

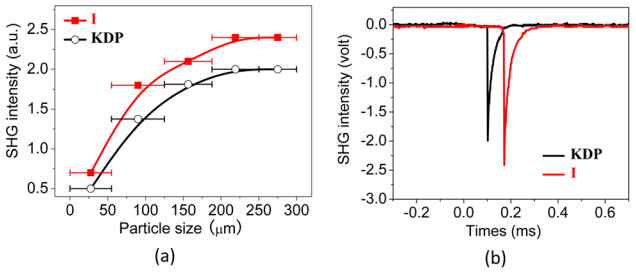

Figure 3. (a) SHG intensity vs particle size curves at 1064 nm. (b) Oscilloscope traces of SHG signals. KDP samples serve as the references. Solid curves in (a) are drawn to guide the eyes and are not fits to the data.

with increasing particle sizes before they attain the maximum independent of the particle sizes, indicating that **I** is phase-matchable at the wavelength of 1064 nm. The oscilloscope traces of SHG signals (Figure 3b) show that the SHG efficiency for **I** is about 1.2 times that of KH_2PO_4 (KDP) in the same particle size of 250−300 μm, which is approximately equal to that of KBBF (~1.24 × KDP).[8c] Such a powder SHG response is also comparable to those of the newly reported beryllium borates, such as β-$KBe_2B_3O_7$ (0.75 × KDP),[10] γ-$KBe_2B_3O_7$ (0.68 × KDP),[10] $RbBe_2B_3O_7$ (0.79 × KDP),[10] $NaBeB_3O_6$ (1.60 × KDP),[10] and $Na_2CsBe_6B_5O_{15}$ (1.17 × KDP)[11] as well as $Na_2Be_4B_4O_{11}$ (1.3 × KDP) and $LiNa_5Be_{12}B_{12}O_{33}$ (1.4 × KDP).[14] Figure S3 shows the UV−vis near-infrared diffuse reflectance spectrum of **I** powders. There is no obvious absorption peak in the range of 6.20−1.13 eV (corresponding to 200−1100 nm), indicating that **I** may have potential use in deep-UV applications.

In order to elucidate the microscopic mechanism of optical properties for **I**, we performed the first-principles calculations by the plane-wave pseudopotential method implemented in the CASTEP package based on the density functional theory.[20] As shown in Figure S4a, **I** is a direct bandgap compound with a bandgap of 6.58 eV (corresponding to 188 nm), which which further confirmed the deep-UV transparency of **I**. According to the density of states and partial density of states projected on the constitutional atoms (see Figure S4b), for crystal **I** it is the $[BO_3]^{3-}$ group that determines the optical properties, e.g., SHG coefficients, whereas the contribution of the *A*-site cations is negligibly small.

The SHG coefficients (d_{ij}) were calculated by the formula developed by Lin et al.[21] Under the restriction of Kleinman's symmetry,[22] **I** has three nonzero independent SHG coefficients owing to its $P3_1c$ space group. The calculated results are d_{22} = 0.39 pm/V, d_{31} = −0.023 pm/V, d_{33} = −0.025 pm/V, respectively. In comparison, the calculated value for KBBF is d_{11} = 0.41 pm/V in the previous work of our coauthors Lin et al.[23] In addition, the strong anisotropy of NLO effects ($d_{22} \gg d_{31}, d_{33}$) explicitly reflects the anisotropic structure feature in **I**, i.e., the infinite 2D $[Al_3(BO_3)_3OF]_\infty$ layer in the *ab* plane has much larger NLO response as compared with the structure along the *c*-axis.

According to the anionic group theory,[24] the overall nonlinearity of a crystal is the geometrical superposition of the microscopic second-order susceptibility of NLO-active anionic groups (e.g., $[BO_3]^{3-}$ groups in **I** and KBBF). Owing to the narrow interlayer spacing distance of 4.37 Å (in comparison, KBBF, 6.25 Å),[8a] **I** exhibits a relatively large spatial density for the $[BO_3]^{3-}$ groups (0.0105 per unit volume), which is about 1.11 times that of KBBF (0.00946 per unit volume). In addition, there is a small acute angle of 35.6(8)° between the orientations of the $[BO_3]^{3-}$ groups in adjacent $[Al_3(BO_3)_3OF]_\infty$ layers of **I**, whereas the $[BO_3]^{3-}$ groups in KBBF are in perfect aligning. Consequently, the overall SHG response of **I** is approximately equal to that of KBBF.

In summary, we have synthesized a new beryllium-free borate $Rb_3Al_3B_3O_{10}F$ by solid-state reaction techniques. This compound features a framework structure that preserves the structural merits of KBBF, resulting in the deep-UV transparency and phase-matchability with the powder SHG efficiency approximately equal to that of KBBF at 1064 nm. Furthermore, $Rb_3Al_3B_3O_{10}F$ exhibits a remarkably strong interayer bonding of more than 9.5 times that of KBBF in magnitude, and thus no layering single-crystal growth tendency was observed. In addition, the crystal is nonhygroscopic and of high thermal stablility. These attributes make $Rb_3Al_3B_3O_{10}F$ a promising deep-UV NLO crystal. Future efforts will be devoted to the growth of bulk single crystals and the characterizations of optical properties for this crystal. It is anticipated that more deep-UV NLO materials with good performance will be developed through the substitution of Be for Al in the beryllium borates.

■ ASSOCIATED CONTENT

Supporting Information

Photograph of **I** crystals, diffuse reflectance absorption curve, crystallographical data (CIF), and additional data. Deposition number CCDC 1038364 for **I**. This material is available free of charge via the Internet at http://pubs.acs.org.

■ AUTHOR INFORMATION

Corresponding Author

*jhluo@fjirsm.ac.cn

Notes

The authors declare no competing financial interest.

■ ACKNOWLEDGMENTS

This work was financially supported by the National Natural Science Foundation of China (21222102, 21373220, 21171166, 11174297, and 11474292), the National Basic Research Project of China (2011CB922204, 2011CB935904), the Natural

DOI: 10.1021/ja5128314
J. Am. Chem. Soc. 2015, 137, 2207−2210

Science Foundation of the Fujian Province (2014J05068), and the opening fund of Key Laboratory of Functional Crystals and Laser Technology, TIPC, CAS (FCLT 201306). S.Z. thanks the support from Chunmiao Project of Haixi Institute of Chinese Academy of Sciences (CMZX-2015-003).

REFERENCES

(1) (a) Franken, P.; Hill, A.; Peters, C.; Weinreich, G. *Phys. Rev. Lett.* **1961**, *7*, 118. (b) Becker, P. *Adv. Mater.* **1998**, *10*, 979. (c) Halasyamani, P. S.; Poeppelmeier, K. R. *Chem. Mater.* **1998**, *10*, 2753. (d) Sasaki, T.; Mori, Y.; Yoshimura, M.; Yap, Y. K.; Kamimura, T. *Mater. Sci. Eng. R-Rep.* **2000**, *30*, 1. (e) Inaguma, Y.; Yoshida, M.; Katsumata, T. *J. Am. Chem. Soc.* **2008**, *130*, 6704. (f) Zhang, J.; Zhang, Z.; Sun, Y.; Zhang, C.; Zhang, S.; Liu, Y.; Tao, X. *J. Mater. Chem.* **2012**, *22*, 9921. (g) Donakowski, M. D.; Gautier, R.; Yeon, J. H.; Moore, D. T.; Nino, J. C.; Halasyamani, P. S.; Poeppelmeier, K. R. *J. Am. Chem. Soc.* **2012**, *134*, 7679. (h) Chung, I.; Kanatzidis, M. G. *Chem. Mater.* **2014**, *26*, 849.

(2) Chen, C. T.; Wu, B. C.; Jiang, A. D.; You, G. M. *Sci. Sin., Ser. B (Engl. Ed.)* **1985**, *28*, 235.

(3) Chen, C. T.; Wu, Y. C.; Jiang, A. D.; Wu, B. C.; You, G. M.; Li, R. K.; Lin, S. J. *J. Opt. Soc. Am. B* **1989**, *6*, 616.

(4) Driscoll, T. A.; Hoffman, H. J.; Stone, R. E.; Perkins, P. E. *J. Opt. Soc. Am. B* **1986**, *3*, 683.

(5) Harasaki, A.; Kato, K. *Jpn. J. Appl. Phys.* **1997**, *36*, 700.

(6) Boyd, G. D.; Buehler, E.; Storz, F. G. *Appl. Phys. Lett.* **1971**, *18*, 301.

(7) Kang, L.; Lin, Z. S.; Qin, J. G.; Chen, C. T. *Sci. Rep.* **2013**, *3*, 1366.

(8) (a) Xia, Y. N.; Chen, C. T.; Tang, D. Y.; Wu, B. C. *Adv. Mater.* **1995**, *7*, 79. (b) Cyranoski, D. *Nature* **2009**, *457*, 953. (c) Chen, C. T.; Wang, G. L.; Wang, X. Y.; Xu, Z. Y. *Appl. Phys. B: Laser Opt.* **2009**, *97*, 9.

(9) Chen, C. T.; Wang, Y. B.; Wu, B. C.; Wu, K. C.; Zeng, W. L.; Yu, L. H. *Nature* **1995**, *373*, 322.

(10) Wang, S. C.; Ye, N.; Li, W.; Zhao, D. *J. Am. Chem. Soc.* **2010**, *132*, 8779.

(11) Wang, S. C.; Ye, N. *J. Am. Chem. Soc.* **2011**, *133*, 11458.

(12) Huang, H. W.; Yao, J. Y.; Lin, Z. S.; Wang, X. Y.; He, R.; Yao, W. J.; Zhai, N. X.; Chen, C. T. *Angew. Chem., Int. Ed. Engl.* **2011**, *50*, 9141.

(13) Huang, H. W.; Yao, J. Y.; Lin, Z.; Wang, X. Y.; He, R.; Yao, W. J.; Zhai, N. X.; Chen, C. T. *Chem. Mater.* **2011**, *23*, 5457.

(14) Huang, H. W.; Liu, L. J.; Jin, S. F.; Yao, W. J.; Zhang, Y. H.; Chen, C. T. *J. Am. Chem. Soc.* **2013**, *135*, 18319.

(15) (a) McMillen, C. D.; Stritzinger, J. T.; Kolis, J. W. *Inorg. Chem.* **2012**, *51*, 3953. (b) Wu, H. P.; Yu, H. W.; Yang, Z. H.; Hou, X. L.; Su, X.; Pan, S. L.; Poeppelmeier, K. R.; Rondinelli, J. M. *J. Am. Chem. Soc.* **2013**, *135*, 4215. (c) Wu, H. P.; Yu, H. W.; Pan, S. L.; Huang, Z. J.; Yang, Z. H.; Su, X.; Poeppelmeier, K. R. *Angew. Chem., Int. Ed. Engl.* **2013**, *52*, 3406. (d) Wu, H.; Pan, S.; Poeppelmeier, K. R.; Li, H.; Jia, D.; Chen, Z.; Fan, X.; Yang, Y.; Rondinelli, J. M.; Luo, H. *J. Am. Chem. Soc.* **2011**, *133*, 7786.

(16) Zhao, S. G.; Gong, P. F.; Bai, L.; Xu, X.; Zhang, S. Q.; Sun, Z. H.; Lin, Z. S.; Hong, M. C.; Chen, C. T.; Luo, J. H. *Nat. Commun.* **2014**, *5*, 4019.

(17) (a) Brown, I. D.; Altermatt, D. *Acta Crystallogr. B* **1985**, *41*, 244. (b) Brese, N. E.; Okeeffe, M. *Acta Crystallogr. B* **1991**, *47*, 192.

(18) Williams, E. R.; Faller, J. E.; Hill, H. A. *Phys. Rev. Lett.* **1971**, *26*, 721.

(19) Kurtz, S. K.; Perry, T. T. *J. Appl. Phys.* **1968**, *39*, 3798.

(20) (a) Kohn, W.; Sham, L. J. *Phys. Rev.* **1965**, *140*, A1133. (b) Payne, M. C.; Teter, M. P.; Allan, D. C.; Arias, T. A.; Joannopoulos, J. D. *Rev. Mod. Phys.* **1992**, *64*, 1045. (c) Clark, S. J.; Segall, M. D.; Pickard, C. J.; Hasnip, P. J.; Probert, M. J.; Refson, K.; Payne, M. C. *Z. Kristallogr.* **2005**, *220*, 567.

(21) (a) Lin, J.; Lee, M. H.; Liu, Z. P.; Chen, C. T.; Pickard, C. J. *Phys. Rev. B* **1999**, *60*, 13380. (b) Lin, Z. S.; Lin, J.; Wang, Z. Z.; Wu, Y. C.; Ye, N.; Chen, C. T.; Li, R. K. *J. Phys.: Condens. Matter* **2001**, *13*, R369.

(22) Kleinman, D. A. *Phys. Rev.* **1962**, *126*, 1977.

(23) Kang, L.; Luo, S. Y.; Huang, H. W.; Zheng, T.; Lin, Z. S.; Chen, C. T. *J. Phys.: Condens. Matter* **2012**, *24*, 330503.

(24) Chen, C. *Sci. Sin.* **1979**, *22*, 756.

DOI: 10.1021/ja5128314
J. Am. Chem. Soc. 2015, 137, 2207−2210